AGU ADVANCING EARTH AND SPACE SCIENCES

Geophysical Research Letters

RESEARCH LETTER
10.1029/2024GL108916

Contrasted Trends in Chlorophyll-*a* Satellite Products

Etienne Pauthenet[1], Elodie Martinez[1], Thomas Gorgues[1], Joana Roussillon[1,2], Lucas Drumetz[3], Ronan Fablet[3], and Maïlys Roux[1,4]

[1]IRD, CNRS, University Brest, Ifremer, Laboratoire d'Océanographie Physique et Spatiale (LOPS), IUEM, Plouzané, France, [2]IRD, Géosciences Environnement Toulouse (GET), UMR5563, CNRS, Université Toulouse 3, Toulouse, France, [3]IMT Atlantique, UMR CNRS LabSTICC, Technopole Brest Iroise, Plouzané, France, [4]École Normale Supérieure, Université Paris Sciences et Lettres, Paris, France

Abstract Phytoplankton sustains marine ecosystems and influences the global carbon cycle. This study analyzes trends in surface chlorophyll-*a* concentration (Schl), a proxy for phytoplankton biomass, using six of the most widely used merged satellite products. Significant regional variations are observed, with contrasting trends observed among different products. To assess if these trends can be related to changes in the environment or to bias in radiometric products, a convolutional neural network is used to examine the relationship between physical ocean variables versus Schl. The results suggest that the merging algorithm of Globcolour-GSM is not reliable for trend detection and that observed changes in Schl after 2012/2016 are not supported by changes of the physical ocean. These results emphasize the need for careful interpretation of satellite-derived Schl trends and highlight the potential of machine learning in understanding the complex interactions in marine ecosystems.

Plain Language Summary This study investigates trends in surface concentration of chlorophyll-*a* (Schl), a proxy of phytoplankton biomass in the ocean. Our study reveals different trends according to the considered satellite products, challenging previous assumptions relating some Schl negative trends to the anthropogenic signal. To investigate the reliability of these trends, a machine learning approach is applied, showing that the observed changes in Schl trends may not always be related to changes in some physical ocean properties but sometimes to sensor drift. These findings underscore the importance of considering multiple factors when interpreting Schl trends and highlight the potential of advanced statistical tools in understanding marine ecosystems.

Key Points:

- An analysis of remotely sensed surface chlorophyll-*a* concentration reveals contrasted trends between available merged products
- A convolutional neural network can effectively reconstruct surface chlorophyll-*a* concentration from the properties of the ocean surface
- Recent trends in surface chlorophyll-*a* concentration merged products are not all supported by changes in properties of the ocean surface

Supporting Information:

Supporting Information may be found in the online version of this article.

Correspondence to:

E. Pauthenet,
etienne.pauthenet@ird.fr

Citation:

Pauthenet, E., Martinez, E., Gorgues, T., Roussillon, J., Drumetz, L., Fablet, R., & Roux, M. (2024). Contrasted trends in chlorophyll-a satellite products. *Geophysical Research Letters*, *51*, e2024GL108916. https://doi.org/10.1029/2024GL108916

Received 22 FEB 2024
Accepted 16 JUL 2024

Author Contributions:

Conceptualization: Etienne Pauthenet, Elodie Martinez, Thomas Gorgues, Lucas Drumetz, Ronan Fablet
Data curation: Etienne Pauthenet, Maïlys Roux
Formal analysis: Etienne Pauthenet, Joana Roussillon, Maïlys Roux
Funding acquisition: Elodie Martinez
Investigation: Etienne Pauthenet, Thomas Gorgues
Methodology: Etienne Pauthenet, Elodie Martinez, Thomas Gorgues, Lucas Drumetz, Ronan Fablet
Project administration: Elodie Martinez
Resources: Elodie Martinez

1. Introduction

Phytoplankton sustains the marine food chain and affects the Earth's climate through its impact on the carbon cycle. Human-induced climate change is responsible for, among others, a temperature increase at global scale and regional modifications of the winds that both impact ocean stratification (IPCC, 2021), and consequently surface nutrient availability for phytoplankton growth. Thus, global phytoplankton biomass is expected to be impacted by these environmental changes (Lotze et al., 2019). Variability and trends of this biomass at the surface of the ocean can be observed over the last 25 years thanks to a proxy, the chlorophyll-*a* surface concentration (Schl) which can be derived from satellite radiometers. Schl is considered as an essential climate variable (ECV) whose measurement contributes to monitor the Earth's climate. However, to quantify the natural variability from the anthropogenic signal on Schl, long enough time-series (about 40 years at a global scale according to Henson et al., 2010) are required. This implies continuous time-series should be created merging several radiometric satellite products without introducing biases, artifacts or discontinuities (Hammond et al., 2017).

Nowadays, several Schl "time-series for climate" exist and they have begun to be used in Schl trends assessment. Some recent studies have notably considered only one multi-sensors product to draw conclusions about Schl trends (e.g., Agarwal et al., 2024; Tian & Zhang, 2023). Indeed, in the latter study, the authors reported a robust decrease of Schl at global scale over the last 25 years. They attributed this decrease to the anthropogenic activity-induced warming whose impacts on ocean forcings reflect on Schl. Yet, a comprehensive comparison of Schl from the different available products is lacking to infer the robustness of one's claim. Here, we therefore propose to investigate to what extent reported Schl trends from a large range of multi-sensor products used by the scientific community have been consistent or not between each other. We also illustrate how Schl reconstructions from physical predictors using a machine learning approach can provide insights into the consistency or possible existing bias in these climate time-series.

Software: Etienne Pauthenet, Joana Roussillon, Lucas Drumetz, Ronan Fablet
Supervision: Elodie Martinez, Thomas Gorgues, Lucas Drumetz, Ronan Fablet
Validation: Etienne Pauthenet
Visualization: Etienne Pauthenet
Writing – original draft: Etienne Pauthenet
Writing – review & editing: Etienne Pauthenet, Elodie Martinez, Thomas Gorgues, Joana Roussillon

Table 1
List of Data Used in This Study, for the Six Schl Merged Products, the Five Schl Mono Sensors and for the Eight Input Features of the Convolutional Neural Network

In text name	File name or preprocessing	Citation
Yu2023	–	Yu et al. (2022)
Multiobs-CMEMS	MULTIOBS-GLO-BIO-BGC-3D-REP-015-010	Sauzède et al. (2021)
OC-CCI	OCEANCOLOUR-GLO-BGC-L3-MY-009-107	ESA et al. (2023)
Globcolour-CMEMS	OCEANCOLOUR-GLO-BGC-L3-MY-009-103	(ACRI-ST et al. (2023)
Globcolour-AVW	–	ACRI-ST (2020a)
Globcolour-GSM	–	ACRI-ST (2020a)
SeaWiFS	GSM and NASA R2018.0	ACRI-ST (2020a)
VIIRS-NPP	GSM and NASA R2018.0	ACRI-ST (2020a)
MODIS AQUA	GSM and NASA R2018.0	ACRI-ST (2020a)
OLCI-A	GSM and ESA PB 2.16 to 2.55	ACRI-ST (2020a)
MERIS	GSM and ESA third preprocessing	ACRI-ST (2020a)
SST	METOFFICE-GLO-SST-L4-REP-OBS-SST	Worsfold et al. (2022)
SLA	SEALEVEL-GLO-PHY-L4-MY-008-047	CLS & Pujol (2023)
U10, V10, SSR	ERA5	Hersbach et al. (2023)
U, V	OSCAR-L4-OC-FINAL-V2.0	Dohan (2021)
MDT	CNES-CLS18	Mulet et al. (2021a)

2. Data

2.1. Radiometric Products of Schl

Schl merged products consist in level-3 global ocean color satellite-derived observations at a daily, 8-day or monthly frequency covering the 1997-09 to 2022-12 time period, and with a 4 km to 0.25° spatial resolution. In the present study, we averaged all products on common temporal and spatial resolution (i.e., monthly frequency and on a 1/4° grid). We focus on Case 1 waters (i.e., by removing regions with bathymetry shallower than 200 m) and mid-latitudes (i.e., 50°S–50°N) as those areas need specific algorithms (Ferreira et al., 2022; Lewis & Arrigo, 2020). The sensors available to build the merged Schl data sets are: SeaWiFS covering the 1997-09 to 2010-12 period, MODIS-Aqua from 2002-07 to present, MERIS from 2002-04 to 2012-04, OLCI-A from 2016-04 to present, and VIIRS-NPP from 2012-01 to present. Six Schl data sets, which merge these different sensors from 1997-09 to today, are used in the present study. The Ocean Color Climate Change Initiative (OC-CCI) product version 6.0 merges level-1 reflectance (except level-2 for SeaWiFS) after a band-shifting and bias-correction to match those from MERIS (Jackson et al., 2022; Sathyendranath et al., 2019). The Globcolour-GSM product also merges inter-sensor reflectance observations using a different atmospheric correction and semi-analytical bio-optical model without inter-mission bias correction (ACRI-ST, 2020b; Maritorena et al., 2010; Maritorena & Siegel, 2005). Globcolour provides two other products based on level-2 weighted averaging Schl (AVW) (O'Reilly et al., 2000). The first one is referred to as Globcolour-AVW, available on the Globcolour website (Table 1). It combines two bio-optical algorithms to derive Schl for oligotrophic waters versus the rest of the ocean. The second one is referred to as the Globcolour-CMEMS, available from the Copernicus marine data store (Garnesson et al., 2019), and adds a third bio-optical algorithms to derive Schl in the mesotrophic and coastal waters. Yu et al. (2023) recently proposed a new data set based on level-2 Schl provided by the NASA and ESA spatial agency, with a different methodology than OC-CCI to correct the inter-sensor bias. Finally, a sixth product is considered and referred to as the Multiobs CMEMS product. Chl is estimated in three-dimension based on physical in situ measurements and satellite surface reflectance from Globcolour-CMEMS and other physical variables thanks to a neural network (Sauzède et al., 2016). We retrieve Schl only from the Multiobs CMEMS.

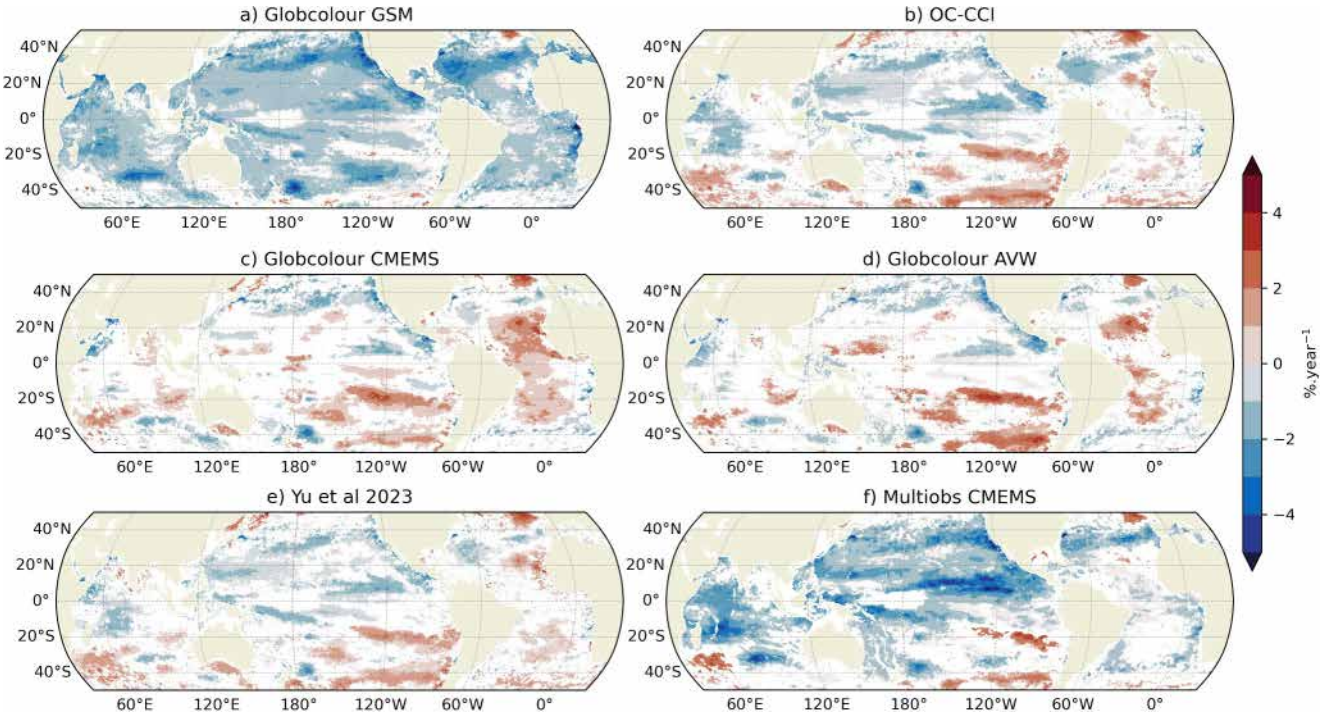

Figure 1. The linear trends of the deseasonalized log-transformed Schl computed for each grid cell show contrasted results depending on the product used. The trends are computed for the period 2002-07 to 2020-12 for the region between 50°S and 50°N and the bathymetry deeper than 200 m. White areas are indicating non-significant trends (p-value >0.05).

2.2. Physical Predictors

To illustrate how reconstructed Schl from physical predictors can provide insights into the consistency or possible existing bias in climate time-series, we model the link between Schl and some physical fields with a neural network (Roussillon et al., 2023). The chosen physical predictors are L4 satellite and reanalysis data, that we interpolate on a 1/4° and monthly grid from 1998 to 01 to 2020-12 (The surface currents data were only available until this date at the time of the study). They are proxy of the main oceanic and atmospheric processes susceptible to provide nutrients to the upper sunlit layer and required for phytoplankton to grow. We use the Sea Level Anomaly (SLA) from CNES-CLS (CLS & Pujol, 2023), the Sea Surface Temperature (SST) from the Met Office (Good et al., 2020), the zonal (U) and meridian (V) components of the surface currents from the Ocean Surface Current Analyses-Real time (OSCAR) product version 2.0 (Dohan, 2021), the wind components at 10 m (U10 and V10), the Surface Shortwave Radiation (SSR) from the ERA reanalysis (Hersbach et al., 2020) and the static field of Mean Dynamic Topography (MDT) from the Centre National d'Etude Spatiale (CNES-CLS18) (Mulet et al., 2021b). Roussillon et al. (2023) do not use the MDT but preliminary sensitivity tests revealed that adding MDT to the predictors improves the Schl reconstruction (Figure S2 in Supporting Information S1).

3. Method

3.1. Trend Analysis

A constant annual cycle is removed before fitting the linear regression for each grid cell, following Vantrepotte and Mélin (2009). While the Schl seasonal cycle might change over time (Henson et al., 2013), removing a changing seasonal cycle with a seasonal-trend decomposition (Cleveland et al., 1990), would bias the trend detection. Maps of trends show the slope of the linear regression for each deseasonalized time series, expressed in % year^{-1} (Figure 1). The p-value for each regression is computed and displayed with white areas for p-value >0.05. Figure 2 shows the spatially weighted median of Schl for multi-sensor products (a) and single-sensors (b). The weighting is done with the cosines of latitude. The median is preferred over the mean to represent the chl-*a* heavy-tailed distribution. The median is more robust to outliers and less affected by skewness, making it easier to interpret (Wasserman, 2013).

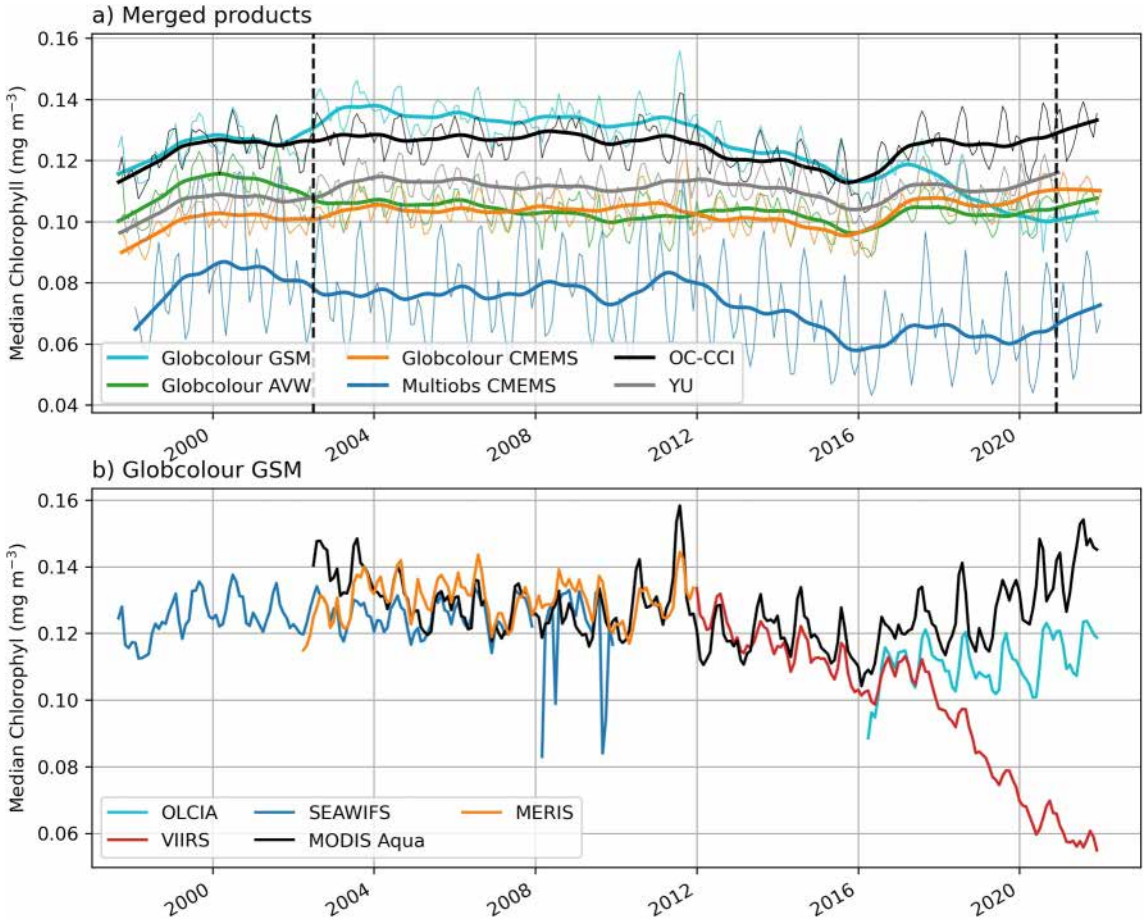

Figure 2. Spatial weighted average of Schl for each merged products (a) and for several sensors reprocessed by Globcolour-GSM (b). The panel (a) displays the median Schl concentration by month (thin line) and smoothed with a locally estimated scatterplot smoothing (loess, thick line). The overall shift between products is mostly due to the different numbers of valid points in each product. Dashed lines are added on panel (a) at 2002-07 and 2020-12, the period of trend showed in Figure 1.

3.2. Convolutional Neural Network

We use a Convolutional Neural Network (CNN) to learn the relationship between physical surface properties and Schl as described as the baseline CNN in Roussillon et al. (2023). It is composed of a sequence of five two-dimensional convolutional layers with 3 × 3 kernel sizes, stride and padding 1 × 1, and with ReLU activations (Figure S3 in Supporting Information S1). A dropout of 20% is set on the last layer to prevent from overfitting (Figure S4 in Supporting Information S1) and the learning rate is set at 0.001. Each CNN is trained for 300 epochs. The input fields used are the physical predictors presented above versus Schl from the different products each in turn. Relationships between the predictors and Schl are firstly trained and validated between 2002-07 and 2009-12, a time period with the same number of radiometric sensors. Then, Schl is reconstructed over the entire time series and tests are performed over the independent 2011-01 to 2020-12 time period (Figure 3 and Figure S5 in Supporting Information S1). The split between the training (80%) and validation (20%) data sets is done with a particular attention that each month is proportionally represented between train and validation. Each CNN configuration is trained/validated/tested 10 times and each monthly median is shown on Figure 3 with the median average as the thick red line. In addition, we also investigate the relationships between the predictors and the mono-sensor Schl from VIIRS. Here, the training and validation data sets are selected between 2012-01 and 2015-12 (Figure 3c). An impressive feature of the CNN Schl reconstruction is its ability to derive gap free Schl, from knowledge of the state of the ocean. However, bias when compared with the satellite Schl can arise from missing values in the observations. Consequently, the mask of missing data is removed from CNN derived Schl before computing the median, to match the values of observed Schl (Figure 3). The ensemble mean is used to

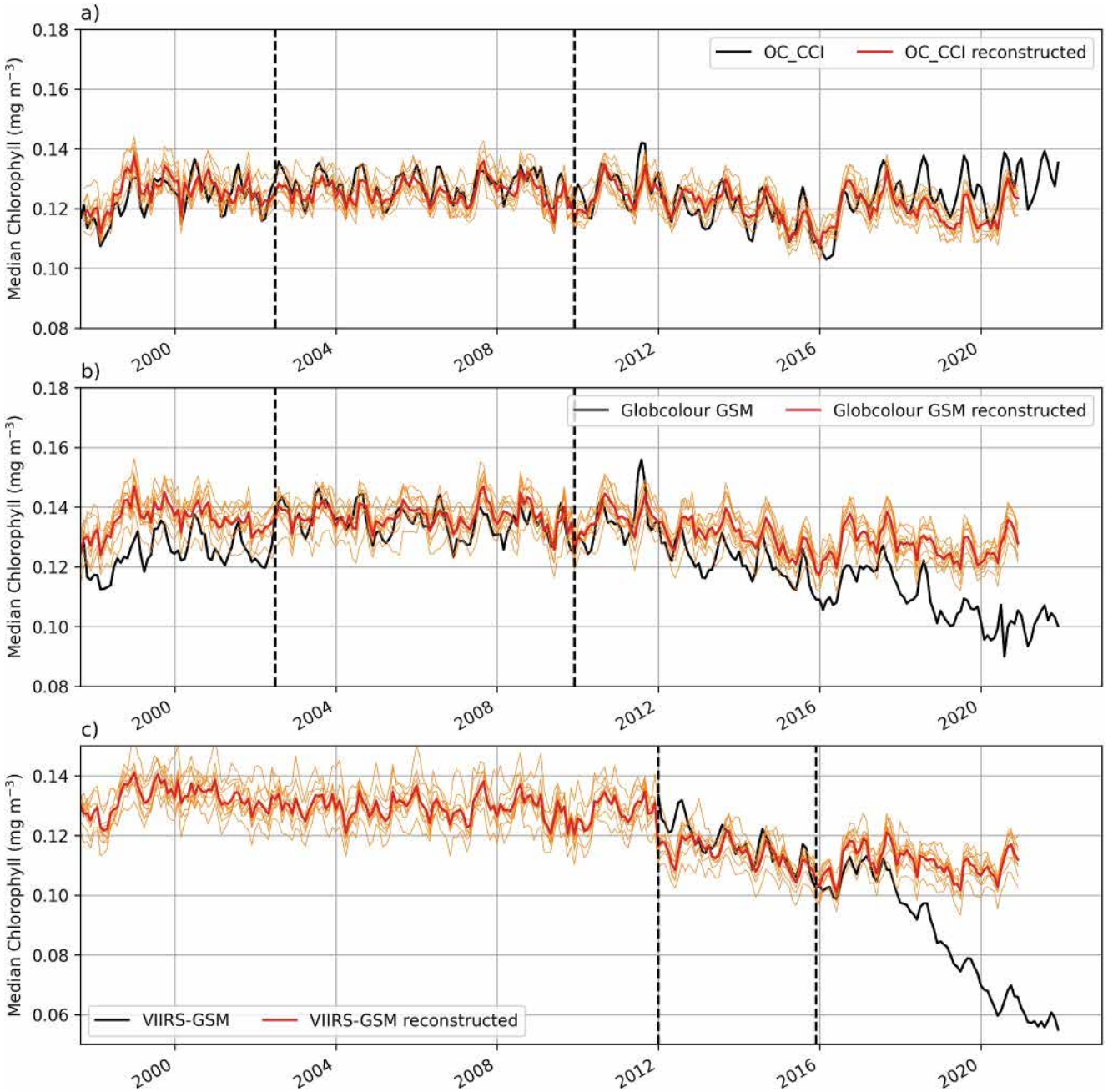

Figure 3. Median Schl for monthly maps reconstructed with a CNN. Each panels shows 10 runs (orange thin lines) and their average (thick red line) together with the median Schl of the observations (thick black line) based on panel (a) OC-CCI and (b) Globcolour-GSM merged products, and (c) the VIIRS sensor processed by GSM. The two vertical dashed lines delineate the training periods. The reconstructed Schl from VIIRS (c) before 2012 appears slightly higher than after 2012, because the mask of missing data is removed to match the observations after 2012, but gap-free fields of Schl are used before 2012 to compute the median.

compute the trends on Figure 4 right column. The codes to train the CNNs and produce the figures are available at https://github.com/ANR-DREAM/Trend_paper/.

4. Results and Discussions

Consistently with Tian and Zhang (2023) who used the Globcolour-GSM merged product, a significant Schl negative trend is here highlighted at a global scale over 2002–2020 (Figure 1a). These authors attributed the underlying process of this Schl decrease to anthropogenic greenhouse emissions leading to a surface warming and

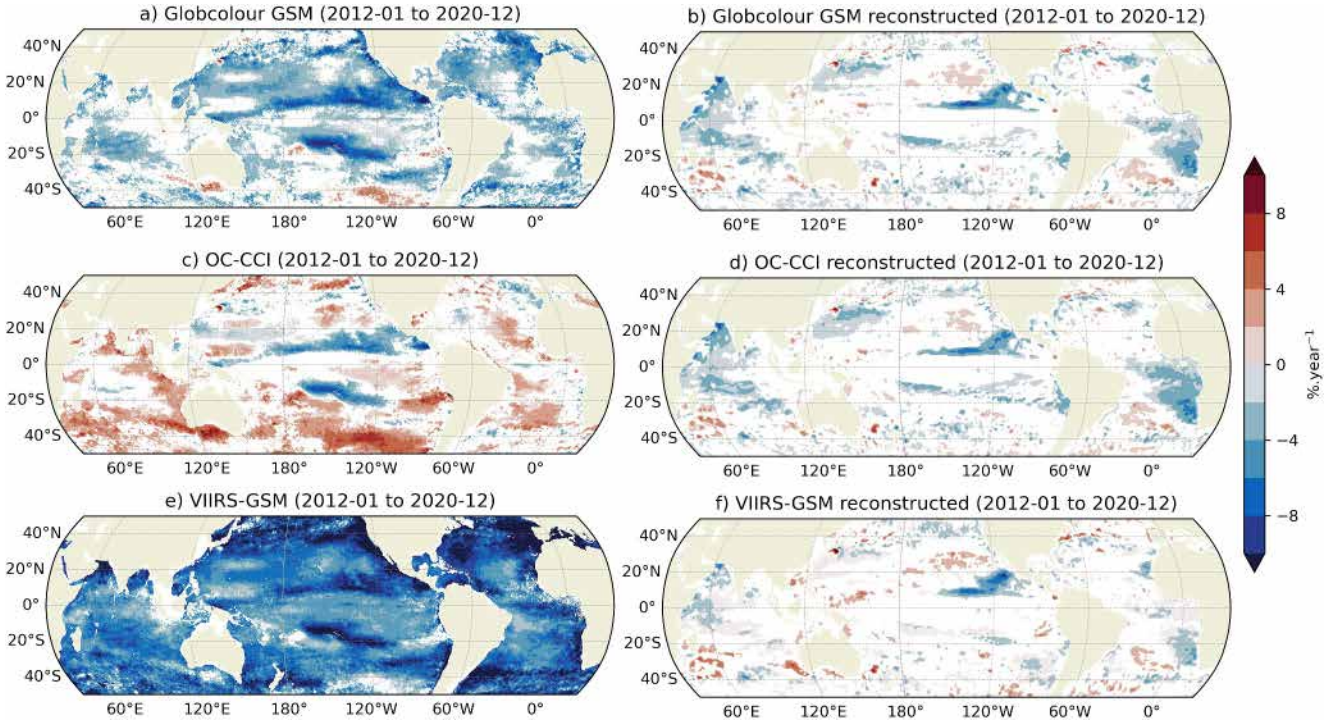

Figure 4. Observed (a, c, e) and reconstructed (b, d, f) trends are not consistent for the period 2012-01 to 2020-12. The linear trends of the deseasonalized log-transformed Schl is computed for each grid cell for the observed Schl (left column) and reconstructed Schl with CNN (right column). The reconstructed maps are averages for 10 model by CNN configuration. The trends are computed for the region between 50°S and 50°N and the bathymetry deeper than 200 m. White areas are indicating non-significant trends (p-value >0.05).

an increase of surface stratification reducing nutrient availability in the surface layer. However, this result appears to be strongly contrasted with the Schl trends computed from four other satellite merged products (namely OC-CCI, Yu2023, Globcolour-CMEMS and Globcolour-AVW). These four products show very similar patterns as they are all partially based on the NASA R2018.0 and ESA reprocessing for their respective sensors, unlike Globcolour-GSM which derives Schl thanks to a specific semi-analytical ocean color model (Maritorena et al., 2002). Considering now the OC-CCI product which is widely used in the ocean color community (e.g., Fowler et al., 2023; van Oostende et al., 2023), a decreasing trend can be observed in the northern and equatorial Pacific Ocean, along the Pacific Intertropical Convergence Zone (ITCZ), the tropical Indian and northern Atlantic Oceans (Figure 1b). However, a significant positive trend of Schl appears in the northern hemisphere for higher latitudes than 40°N and in the Southern Ocean generally south of the Subtropical Front (Graham & Boer, 2013), as well as in the south-eastern Pacific. Schl also significantly increases for most of the Atlantic Ocean. The Yu2023 and the two Globcolour-CMEMS and Globcolour-AVW products (Figures 1c–1e) show Schl trends close to the OC-CCI ones although the amplitudes may be slightly regionally different or with opposite sign for the two Globcolour products mostly in the subtropical western Pacific and Arabian Sea. Finally, the Multiobs-CMEMS product (Figure 1f) reveals similar pattern than OC-CCI but with stronger negative amplitude in the north Pacific particularly along the ITCZ ($<-5\%$ year^{-1}). Little to no significant positive trends are visible in the Southern and Atlantic Ocean which contrasts greatly with the strong positive trends in the four previous products (Figures 1b–1e). This is likely due to differences in the methodology and data sets used to derive Schl for the Multiobs-CMEMS product.

To investigate these contrasted trends along time, the spatially weighted median of Schl is computed for the six merged products (Figure 2a). Time series are known to be impacted by the number of satellite sensors on the global Schl trends and four sub-periods are identified (see Figure 4 in van Oostende et al., 2022). First, the 1997-09 to 2002-07 period relies on the SeaWiFS sensor only. Then MODIS, MERIS and SeaWiFS sensors cover the period 2002-07 to 2010-12. The third period is made of MODIS and VIIRS from 2012-01 to 2015-09. Finally, from 2016-05 OLCI completes VIIRS and MODIS until 2020-12. Thus, the different amount of available observations within each product (Figure S1 in Supporting Information S1) can partially explain the range of

observed variability between each time-period (Figure 2a). The Multiobs-CMEMS product is lower when compared to the others, likely due to the difference in the methodology used to derive Schl as mentioned above. Most of all, the six products present similar trends over the three first sub-periods (i.e., until 2016). Then, Globcolour-GSM (Figure 2a, blue) diverges from the five others with a clear decrease in Schl. Because the five merged products except Globcolour-GSM have a common basis to derive Schl (i.e., part of the same reprocessing), it cannot be stated that Globcolour-GSM is unreliable rather than the other products for a computable reason. Thus, we investigate the median Schl for the different sensors used in the Globcolour-GSM product (Figure 2b). The time-variability is relatively close between the different sensors between 2002 and 2012. Then, the Schl decrease in VIIRS is more pronounced than for the other sensors, and from 2016 it starts to dramatically diverge with an even stronger Schl decrease versus an increase of MODIS Schl while OLCI-A Schl stays relatively steady. This finding is confirmed on the spatial patterns of the trends between the different Schl products which are all very close over 2002–2011 (Figure S6 in Supporting Information S1) and differ over 2012–2020 (Figure S7 in Supporting Information S1).

To provide insights into the consistency of inter-mission time series and help the interpretation of Schl trends and variability from merged data sets, here we learn relationships between physical predictors likely related to nutrient input within the upper sunlit layer versus Schl from the different radiometric products (black lines in Figure 3). The training is performed over 2002-07 to 2009-12 when learning on merged products (Figures 3a and 3b) and Schl is reconstructed over the entire time-series (red lines in Figure 3). Because results are relatively close when performed on OC-CCI, Yu2023 and Globcolour-CMEMS or AVW (not shown), here we only present those resulting from OC-CCI (Figure 3a) and the contrasted Globcolour-GSM product (Figure 3b). The Schl reconstruction based on OC-CCI closely matches the observations (Figure 3a), even outside the training period. The decreasing trend over 2012–2016 is also reproduced as well as the plateau since 2016. However the seasonal high values are underestimated after 2018, likely linked to a bias in the MODIS sensor already reported but which was only partially corrected in the NASA R2018.0 reprocessing (Figure 54 in Garnesson et al., 2023). For Globcolour-GSM (Figure 3b), the observed Schl is well reconstructed during the training period. Reconstructed values are higher than observations over the SeaWiFS period. This is consistent with a bias due to a smaller number of observations when compared to the rest of the time-series, and the fact that there is no bias inter-sensor correction in GSM, unlike in the OC-CCI product. The ability of the CNN to highlight some bias in the observations is also apparent when considering the reconstructed Schl which does not reproduce the decreasing trend after the incorporation of the VIIRS sensor in 2012. Finally, we also apply this approach on the VIIRS Schl with a training over the apparently most stable period (i.e., 2012-01 to 2015-12, Figure 3c). Here again, the average median (in red) agrees well with the observations for the training period, but does not reconstruct the strong decreasing trend after 2016 which confirms once again a bias in the data rather than Schl natural variability.

To investigate further the behavior of the reconstructed Schl fields, we compute their trends for selected period of time and compare them with those from the actual Schl products, for the OC-CCI and the contrasted Globcolour-GSM (Figure 4; Figures S6–S8 in Supporting Information S1). The spatial patterns of the 2002-07 to 2011-12 observed trends are similar between the two merged products as presented above, and they are also globally well reproduced by our CNN (Figures S6a and S6b in Supporting Information S1 vs. Figure S8 in Supporting Information S1). Consistently with the period of disagreement between OC-CCI and Globcolour-GSM Schl time-series after 2012 (Figures 2a, 3a, and 3b), the Schl spatial patterns of trends from 201201 to 2020-12 also strongly differ between the two observed products (Figures 4a and 4c). The spatial patterns of trends of VIIRS over 2012–2020 reveal unequivocal decrease of Schl (Figure 4e). The right column of Figure 4 shows the trend for the same period computed from the CNN reconstruction, trained on each product respectively. Interestingly, the three reconstructed trend maps (Figures 4b, 4d, and 4f) are very similar even though they are trained on different data sets. This highlights a consistency in the Schl trends driven by natural induced variability versus a sensor induced bias.

5. Conclusion

Here we investigate Schl trends over the last 23 years from six merged product, five from radiometric observations only and one primarily based on in situ observations (Multiobs-CMEMS). There are good agreements in the large regions of decrease or increase of Schl trends between OC-CCI, Yu2023, Multiobs-CMEMS, Globcolour-CMEMS and Globcolour-AVW, which have some common ground related to the NASA R2018 processing. Meanwhile Globcolour-GSM displays a negative global Schl trend, not present in any other merged

product. The discrepancy between Globcolour-GSM and the four other purely radiometric derived products emerges when the VIIRS sensor is embedded in the Globcolour-GSM time series. Our results bring a new perspective to studies using only one merged product to assess and explain global Schl trend (e.g., Agarwal et al., 2024; Tian & Zhang, 2023). Care should also be taken when analyzing the spatio-temporal patterns of such trends, as biases such as the one reported here in Globcolour-GSM may lead to hasty conclusions. For example, Tian and Zhang (2023) concluded that the impact of the anthropogenic forcing has emerged in the marine ecosystems faster of what was previously reported in the literature, that is, about 40 years for an emerging detectable signal at a global scale (Henson et al., 2010). Inconsistencies between missions have been recognized as a significant challenge to overcome in order to construct climate-quality time series. Yet, long enough time series are necessary to detect such inconsistencies, then additional time (i.e., years) is required to first correct them by the spatial agencies, and second to incorporate these changes in the merged products. In a second part of our work, we propose a machine learning approach to provide quick insights in the consistency (or not) of inter-mission time-series. In addition, such machine learning approaches can help to interpret Schl trends and variability from the merged data sets according to changes of the physical ocean. From radiometric observations, Schl from Glocolour-GSM appears to be strongly impacted by the embedding of the uncanny trend of VIIRS after 2012/2016, while questions arise at the end of the OC-CCI time-series with a Schl increasing likely due to bias from MODIS. Both these decreasing and increasing in Schl recent trends are not reproduced by the CNN reconstructions based on physical predictors and are distributed evenly on the global ocean (Figure S7 in Supporting Information S1). This strongly suggests that the changes in the physical state of the ocean does not explain these Schl trends which are rather related to bias in the radiometric products. Thus, our results advocate for a careful use of Schl radiometric products for trend detection, especially in the recent years and highlight the potential of advanced statistical tools in monitoring marine ecosystems evolution.

Acronyms

CNN	Convolutional Neural Network
GSM	Garver, Siegel, Maritorena model
MERIS	Medium Resolution Imaging Spectrometer
MODIS	Moderate Resolution Imaging Spectroradiometer
MDT	Mean Dynamic Topography
OC-CCI	Ocean Color - Climate Change Initiative
OLCI	Ocean and Land Color Instrument
SeaWiFS	Sea-viewing Wide Field of view Sensor
Schl	Surface chlorophyll-*a*
SST	Sea Surface Temperature
SSR	Surface Solar Radiation
SLA	Sea Level Anomaly
U, V	Zonal and meridional surface velocity
U10, V10	10 m zonal and meridional component of wind
VIIRS	Visible Infrared Imaging Radiometer Suite

Data Availability Statement

The list of data used in this study and its availability is provided in Table 1. The codes to train the CNNs and produce the figures are available at https://github.com/ANR-DREAM/Trend_paper/.

Acknowledgments
This research was funded in part by the Agence Nationale de la Recherche (ANR) under the project ANR-22-CE56-0002-01, and by CNES under Identifiant Action number 8692 within the framework of the ANAPAIS project.

References

ACRI-ST. (2020a). Globcolour chlorophyll concentration for case 1 waters AVW, GSM [Dataset]. *Author*. Retrieved from https://hermes.acri.fr
ACRI-ST. (2020b). *Globcolour product user guide 4.2.1*. (Tech. Rep.). Author.
ACRI-ST, Colella, S., Böhm, E., Cesarini, C., Garnesson, P., Netting, J., & Calton, B. (2023). Global ocean colour (copernicus-globcolour), bio-geo-chemical, l3 (daily) from satellite observations (1997-ongoing) [Dataset]. *E.U. Copernicus Marine Service Information (CMEMS). Marine Data Store (MDS)*. https://doi.org/10.48670/moi-00280
Agarwal, V., Chávez-Casillas, J., Inomura, K., & Mouw, C. B. (2024). Patterns in the temporal complexity of global chlorophyll concentration. *Nature Communications*, *15*(1), 1–8. https://doi.org/10.1038/s41467-024-45976-8
Cleveland, R. B., Cleveland, W. S., McRae, J. E., & Terpenning, I. (1990). Stl: A seasonal-trend decomposition. *Journal of Official Statistics*, *6*(1), 3–73.
CLS, & Pujol, M.-I. (2023). Global ocean gridded l 4 sea surface heights and derived variables reprocessed 1993 ongoing [Dataset]. *E.U. Copernicus Marine Service Information (CMEMS). Marine Data Store (MDS)*. https://doi.org/10.48670/moi-00148
Dohan, K. (2021). Ocean surface current analyses real-time (OSCAR) surface currents - Final 0.25 degree (version 2.0). *NASA Physical Oceanography Distributed Active Archive Center*. https://doi.org/10.5067/OSCAR-25F20
ESA, Colella, S., Böhm, E., Cesarini, C., Garnesson, P., Netting, J., & Calton, B. (2023). Global ocean colour plankton and Reflectances my l3 daily observations [Dataset]. *E.U. Copernicus Marine Service Information (CMEMS). Marine Data Store (MDS)*. https://doi.org/10.48670/moi-00282
Ferreira, A., Brito, A. C., Mendes, C. R., Brotas, V., Costa, R. R., Guerreiro, C. V., et al. (2022). OC4-SO: A new chlorophyll-a algorithm for the western Antarctic peninsula using multi-sensor satellite data. *Remote Sensing*, *14*(5), 1052. https://doi.org/10.3390/rs14051052
Fowler, A. M., Skákala, J., & Ford, D. (2023). Validating and improving the uncertainty assumptions for the assimilation of ocean-colour-derived chlorophyll a into a marine biogeochemistry model of the northwest European shelf seas. *Quarterly Journal of the Royal Meteorological Society*, *149*(750), 300–324. https://doi.org/10.1002/qj.4408
Garnesson, P., Mangin, A., Bretagnon, M., & Jutard, Q. (2023). Satellite observation copernicus-globcolour products (cmems-oc-quid-009-101to104-111-113-116-118). (Tech. Rep.). Copernicus Marine Service: Quality Information Document.
Garnesson, P., Mangin, A., Fanton d'Andon, O., Demaria, J., & Bretagnon, M. (2019). The CMEMS GlobColour chlorophyll a product based on satellite observation: Multi-sensor merging and flagging strategies. *Ocean Science*, *15*(3), 819–830. https://doi.org/10.5194/os-15-819-2019
Good, S., Fiedler, E., Mao, C., Martin, M. J., Maycock, A., Reid, R., et al. (2020). The current configuration of the ostia system for operational production of foundation sea surface temperature and ice concentration analyses. *Remote Sensing*, *12*(4), 720. https://doi.org/10.3390/rs12040720
Graham, R. M., & Boer, A. M. (2013). The dynamical subtropical front. *Journal of Geophysical Research: Oceans*, *118*(10), 5676–5685. https://doi.org/10.1002/jgrc.20408
Hammond, M. L., Beaulieu, C., Sahu, S. K., & Henson, S. A. (2017). Assessing trends and uncertainties in satellite-era ocean chlorophyll using space-time modeling. *Global Biogeochemical Cycles*, *31*(7), 1103–1117. https://doi.org/10.1002/2016gb005600
Henson, S. A., Cole, H., Beaulieu, C., & Yool, A. (2013). The impact of global warming on seasonality of ocean primary production. *Biogeosciences*, *10*(6), 4357–4369. https://doi.org/10.5194/bg-10-4357-2013
Henson, S. A., Sarmiento, J. L., Dunne, J. P., Bopp, L., Lima, I., Doney, S. C., et al. (2010). Detection of anthropogenic climate change in satellite records of ocean chlorophyll and productivity. *Biogeosciences*, *7*(2), 621–640. https://doi.org/10.5194/bg-7-621-2010
Hersbach, H., Bell, B., Berrisford, P., Biavati, G., Horányi, A., Muñoz Sabater, J., et al. (2023). ERA5 hourly data on single levels from 1940 to present [Dataset]. *Copernicus Climate Change Service (C3S) Climate Data Store (CDS)*. https://doi.org/10.24381/cds.adbb2d47
Hersbach, H., Bell, B., Berrisford, P., Hirahara, S., Horányi, A., Muñoz-Sabater, J., et al. (2020). The era5 global reanalysis. *Quarterly Journal of the Royal Meteorological Society*, *146*(730), 1999–2049. https://doi.org/10.1002/qj.3803
IPCC. (2021). Ocean, cryosphere and sea level change [Book Section]. In V. Masson-Delmotte (Ed.), et al. (Eds.), *Climate change 2021: The physical science basis. Contribution of working group i to the sixth assessment report of the intergovernmental panel on climate change* (pp. 1211–1362). Cambridge University Press. https://doi.org/10.1017/9781009157896.011
Jackson, T., Sathyendranath, S., Groom, S., & Calton, B. (2022). *Ocean colour climate change initiative (OC CCI), phase 3, issue 6.1*. (Tech. Rep.). Plymouth Marine Laboratory (PML).
Lewis, K., & Arrigo, K. (2020). Ocean color algorithms for estimating chlorophyll a, CDOM absorption, and particle backscattering in the Arctic Ocean. *Journal of Geophysical Research: Oceans*, *125*(6), e2019JC015706. https://doi.org/10.1029/2019jc015706
Lotze, H. K., Tittensor, D. P., Bryndum-Buchholz, A., Eddy, T. D., Cheung, W. W., Galbraith, E. D., et al. (2019). Global ensemble projections reveal trophic amplification of ocean biomass declines with climate change. *Proceedings of the National Academy of Sciences*, *116*(26), 12907–12912. https://doi.org/10.1073/pnas.1900194116
Maritorena, S., d'Andon, O. H. F., Mangin, A., & Siegel, D. A. (2010). Merged satellite ocean color data products using a bio-optical model: Characteristics, benefits and issues. *Remote Sensing of Environment*, *114*(8), 1791–1804. https://doi.org/10.1016/j.rse.2010.04.002
Maritorena, S., & Siegel, D. A. (2005). Consistent merging of satellite ocean color data sets using a bio-optical model. *Remote Sensing of Environment*, *94*(4), 429–440. https://doi.org/10.1016/j.rse.2004.08.014
Maritorena, S., Siegel, D. A., & Peterson, A. R. (2002). Optimization of a semianalytical ocean color model for global-scale applications. *Applied Optics*, *41*(15), 2705–2714. https://doi.org/10.1364/ao.41.002705
Mulet, S., Rio, M.-H., Etienne, H., Artana, C., Cancet, M., Dibarboure, G., et al. (2021b). The new CNES-CLS18 global mean dynamic topography. *Ocean Science*, *17*(3), 789–808. https://doi.org/10.5194/os-17-789-2021
Mulet, S., Rio, M.-H., Etienne, H., Artana, C., Cancet, M., Dibarboure, G., et al. (2021a). Combined mean dynamic topography—MDT CNES-CLS18 [Dataset]. *Aviso*. Retrieved from https://www.aviso.altimetry.fr/en/data/products/auxiliary-products/mdt/mdt-global-cnes-cls18.html
O'Reilly, J. E., Maritorena, S., Siegel, D. A., O'Brien, M. C., Toole, D., Mitchell, B. G., et al. (2000). Ocean color chlorophyll a algorithms for SeaWIFS, OC2, and OC4: Version 4. SeaWiFS postlaunch calibration and validation analyses. *Part*, *3*, 9–23.
Roussillon, J., Fablet, R., Gorgues, T., Drumetz, L., Littaye, J., & Martinez, E. (2023). A multi-mode convolutional neural network to reconstruct satellite-derived chlorophyll-a time series in the global ocean from physical drivers. *Frontiers in Marine Science*, *10*, 1077623. https://doi.org/10.3389/fmars.2023.1077623
Sathyendranath, S., Brewin, R. J., Brockmann, C., Brotas, V., Calton, B., Chuprin, A., et al. (2019). An ocean-Colour time series for use in climate studies: The experience of the ocean-colour climate change initiative (OC-CCI). *Sensors*, *19*(19), 4285. https://doi.org/10.3390/s19194285
Sauzède, R., Claustre, H., Uitz, J., Jamet, C., Dall'Olmo, G., d'Ortenzio, F., et al. (2016). A neural network-based method for merging ocean color and ARGO data to extend surface bio-optical properties to depth: Retrieval of the particulate backscattering coefficient. *Journal of Geophysical Research: Oceans*, *121*(4), 2552–2571. https://doi.org/10.1002/2015jc011408

Sauzède, R., Renosh, P., & Claustre, H. (2021). Global Ocean 3D chlorophyll-a concentration, particulate backscattering coefficient and particulate organic carbon [Dataset]. *E.U. Copernicus Marine Service Information (CMEMS). Marine Data Store (MDS)*. https://doi.org/10.48670/moi-00046

Tian, F., & Zhang, R.-H. (2023). Decreasing surface chlorophyll in the tropical ocean as an indicator of anthropogenic greenhouse effect during 1998–2020. *Environmental Research Letters*, *18*(8), 084019. https://doi.org/10.1088/1748-9326/ace638

van Oostende, M., Hieronymi, M., Krasemann, H., & Baschek, B. (2023). Global ocean colour trends in biogeochemical provinces. *Frontiers in Marine Science*, *10*, 1052166. https://doi.org/10.3389/fmars.2023.1052166

van Oostende, M., Hieronymi, M., Krasemann, H., Baschek, B., & Röttgers, R. (2022). Correction of inter-mission inconsistencies in merged ocean colour satellite data. *Frontiers in Remote Sensing*, *3*, 882418.

Vantrepotte, V., & Mélin, F. (2009). Temporal variability of 10-year global SeaWIFS time-series of phytoplankton chlorophyll a concentration. *ICES Journal of Marine Science*, *66*(7), 1547–1556. https://doi.org/10.1093/icesjms/fsp107

Wasserman, L. (2013). *All of statistics: A concise course in statistical inference*. Springer Science & Business Media.

Worsfold, M., Good, S., Martin, M., McLaren, A., Roberts-Jones, J., Fiedler, E., & Met Office, U. (2022). Global Ocean OSTIA sea surface temperature and sea ice reprocessed [Dataset]. *E.U. Copernicus Marine Service Information (CMEMS). Marine Data Store (MDS)*. https://doi.org/10.48670/moi-00168

Yu, S., Bai, Y., He, X., Gong, F., & Li, T. (2022). A new merged dataset of global ocean chlorophyll-a concentration for better trend detection (monthly v1.0) [Dataset]. *Zenodo*. https://doi.org/10.5281/zenodo.7092220

Yu, S., Bai, Y., He, X., Li, T., & Gong, F. (2023). A new merged dataset of global ocean chlorophyll-a concentration for better trend detection. *Frontiers in Marine Science*, *10*, 48. https://doi.org/10.3389/fmars.2023.1051619